Size effects of micron-scaled metals – the search continues for materials containing real microstructures[§]

A.H.W. Ngan[1,*], X.X. Chen[1,2], P.S.S. Leung[1,2], R. Gu[1,3] and K.F. Gan[1]

[1] *Department of Mechanical Engineering, The University of Hong Kong, Pokfulam Road, Hong Kong, P.R. China*

[2] *Now at Ove Arup & Partners Hong Kong Ltd, Hong Kong, P.R. China*

[3] *Now at Public Testing & Analysis Center, South University of Science and Technology of China, Shenzhen, P.R. China*

[*]Corresponding Author (hwngan@hku.hk)

§ Perspective article for MRS Communications, invited by Editor and Dr. Neville Moody, based on invited presentation titled "Size effects of metals with real microstructures" at 2016 MRS Fall Meeting.

Abstract

Recent observations on strength and deformation of small metals containing microstructures including dislocation patterns, grain boundaries and second-phase precipitates are reviewed. These microstructures impose an internal length scale that may interplay with the extrinsic length scale due to the specimen size to affect strength and deformation in an intricate manner. For micro-crystals containing pre-existing dislocations, Taylor work-hardening may dictate the dependence of strength on specimen size. The presence of grain boundaries in a small specimen may lead to effects far from the conventional Hall-Petch behavior. Precipitate-dislocation interactions in a small specimen may lead to an interesting weakest-size behavior.

Keywords: Size effect; yield strength; dislocations; precipitates; grain boundaries

1. Introduction

The last decade has seen a surge of research efforts on the effects of specimen size on the strength and deformation of single-crystal, monolithic metals in the micron size regime. Notable observations include the power-law dependence of yield strength on size [1, 2], with a great deal of insights gained into the nucleation of dislocations from a hitherto dislocation-free state [3, 4], deformation under a continuous dislocation-starved state [5-7], stochastic deformation [8-11], and so on. It is by now well known that for crystal sizes ranging from about 1 micron to tens of microns, the yield strength σ_y roughly obeys a power-law variation with respect to specimen size D:

$$\sigma_y \sim D^{-m} \tag{1}$$

where m typically varies between 0.5 and 1 [1, 2]. Thanks to efforts on discrete dislocation dynamics (DDD) simulations [8, 12-17], the decreasing trend of σ_y with D in this regime has now been shown to be due to the group interactions of dislocations in a limited crystal volume, and specifically, the operation of half Frank-Read sources [8, 12, 13], which are Frank-Read sources truncated by the free surface of the specimen. A decreasing trend of σ_y with D can be understood as the consequence of a scaling between the length of such half Frank-Read sources and the specimen size [8, 12, 13].

In the size regime of less than a fraction of a micron or so, tremendous efforts of *in situ* electron microscopy have been made to understand the strength and deformation of various materials [7, 18, 19]. For FCC metals, the results generally point to the difficulty in storing dislocations, i.e. the so-called dislocation starvation condition, in this size regime [5, 6]. Strength in this regime is therefore controlled by the continuous need to nucleate new dislocations, while old ones zip out of the small crystal volume without encountering much difficulty. In this regime, the strength data usually scatter significantly, making it difficult to draw clear-cut conclusions on whether strength varies with size [20, 21], although theoretically, it has been predicted that a weak size effect should exist, due to the expectation that a smaller specimen should contain fewer potential sites for dislocation nucleation [3, 4]. For pristine BCC crystals with a low dislocation content, strength in this regime often approaches the ideal strength limit of about 10% of the elastic modulus, but flow instability in the form of sudden plastic collapse occurs immediately after the onset of yielding [22]. Mechanistically, molecular dynamics have shown that a dislocation starved state is not achieved in submicron BCC crystals due to the frequent cross-slip, or pencil glide, of screw segments of dislocations in this crystal structure, making dislocations difficult to zip out of the crystal volume [23].

From the quick survey above, tremendous progress has been made in the past decade, on the understanding of small-scale plasticity. However, the knowledge database gathered so far has been limited to metals with a monolithic, single crystalline microstructure. Materials for real applications often contain more complex microstructures including dislocation networks or patterns (e.g. subcells), grain boundaries, precipitates, and so on. These microstructures are

often associated with their own characteristic length scales, such as the spacing between dislocations or precipitates, grain or dislocation subcell size, etc. For bulk pieces of specimens with dimensions much larger than the microstructural length scale, strength and deformation will be governed by the microstructural length scale alone, according to well established laws such as Taylor work hardening, where flow stress is inversely proportional to dislocation spacing, the Orowan looping mechanism where precipitation hardening varies inversely with the precipitate spacing, the Hall-Petch relation where strength varies with the inverse of the square-root of grain size, or inverse Hall-Petch behavior for nanocrystalline materials where strength decreases with decreasing grain size in the nanometric range. However, when the specimen size is also in the micron regime, the internal (microstructural) length scale also be in the same size regime as the external (specimen size) length scale, and then the two length scales (external and internal) may couple together [24] to result in interesting effects on strength and deformation unseen before. While this would seem obvious, the literature is still critically short of such information and knowledge. The present authors have recently studied such coupled effects of external and internal lengths scales for some representative types of microstructures, and it is the aim of the present article to summarize the relevant findings, in order to show the magnitude of the problem.

2. Dislocation Microstructures

The first type of microstructure discussed is that due to the pre-existing dislocations themselves. For this, we limit ourselves to situations where dislocation storage can occur effectively, and, as mentioned above, this would be the case for specimen sizes typically larger than ~ 1 micron. In this case, eqn. (1) generally holds, but recent experiments and DDD simulations have shown that the stress exponent *m* is quite sensitive to the initial dislocation content in the crystal [25-30].

To explain why the size dependence has to follow the very simple power law in eqn. (1), and what governs the value of *m*, we proposed a simple, analytical theory [25, 26]. The starting premise is that, in a situation where dislocation storage and hence mutual interactions are possible, strength is controlled by Taylor hardening. Experimental support for this is provided by residual dislocation-density measurement from deformed micro-pillars, as shown in Fig. 1. Here, means including coating and pre-straining of the micro-pillars were used to mediate the initial dislocation contents and their escape from the crystal volume during compressive deformation [31]. For a larger size (5.6 μm) of micro-pillars (Fig. 1(a)), the proof strength of the pillars exhibited excellent scaling with the square-root of the measured density of the residual dislocations in the pillars, indicating that strength of this pillar size is dominated by the Taylor interaction mechanism. However, for a smaller pillar size of ~ 1 μm (Fig. 1(b)), there is no clear trend between proof strength and residual dislocation density, and in fact, the residual dislocation density remained at a lower level not significantly changeable by the means of pre-straining or pillar coating.

Thus, for the case when dislocation storage happens and strength is dominated by Taylor hardening, we are compelled by experimental evidence to consider a dislocation network in which dislocation segments become mobile if the applied stress σ is larger than the segment mobile stress $\sigma_s \sim \mu b/L$, where L is the segment length and other terms have their usual meanings. Out of such a "master" dislocation microstructure (say, a given one in Fig. 2), specimens of different micro-volumes are cropped, and since the specimen size is comparable to the internal length scale L which itself is non-uniform in the master microstructure, the micro-specimens exhibit different strength. In addition to such an assumed picture, we make two further, soft assumptions: (1) the dislocation network of the master microstructure is a fractal of dimension *q*, so that the dislocation mesh length L is statistically distributed as ~ $1/L^q$ (Fig. 3(a)); (2) the dislocation velocity obeys a simple, empirical law $v \sim \sigma^n$.

Thus, for a volume $\sim D^3$ harvested from the master microstructure, the number of mobile dislocation segments under a current applied stress σ would be $\propto D^3 \times \int_0^\sigma p(\sigma_s) d\sigma_s \propto D^3\sigma^{q-1}/(q-1)$, where $p(\sigma_s)$ is the probability distribution function of the mobilization stress σ_s of dislocation segments given by $p(\sigma_s) \sim |dL/d\sigma_s|/L^q \sim \sigma_s^{q-2}$, due to the Taylor hardening law as well as assumption (1) above. Then, for a large ensemble of micro-specimens of the same volume D^3 subject to loading at a constant stress rate $\dot{\sigma}$, the ensemble yielding rate (i.e. the fraction of specimens yielded per unit time) is

$$\dot{N} \sim v \times \frac{D^3\sigma^{q-1}}{(q-1)} = \alpha \frac{D^3\sigma^{q+n-1}}{(q-1)} \tag{2}$$

where v is dislocation velocity and α is a constant. At a current stress level σ, the survivability (without yielding) of the specimens in the ensemble is therefore

$$F(\sigma) = \exp\left[-\frac{1}{\dot{\sigma}}\int_0^\sigma \dot{N}(\sigma')d\sigma'\right] = \exp\left[-\frac{\alpha}{\dot{\sigma}(q+n)(q-1)} D^3\sigma^{q+n}\right] \tag{3}$$

At a given *F* (say, 50%), eqn. (3) requires $D^3\sigma^{q+n}$ to be constant, thus giving

$$\sigma \sim D^{-m} \text{ where } m = 3/(q+n) \tag{4}$$

Eqn. (1) is now proven, and the size exponent *m* is now understood to be inversely related to the fractal dimension *q* of the master dislocation microstructure, as well as the stress exponent *n* of the dislocation velocity. Interestingly, for 3D fractals, $2 < q < 3$, and since $0 < n < \infty$, m is bounded as $0 < m < 1.5$. This tallies with the fact that so far, no experimental report has concluded an m value higher than 1.5.

Eqn. (4) indicates that, unlike what is commonly assumed in the literature, the size exponent m is not a material parameter, but instead, it depends on the initial dislocation structure of the master microstructure from which the micro-specimens are harvested. Further evidence for eqn. (4) was provided by the pre-straining experiments shown in Figs. 2 and 3 [26]. Here, micropillars were focused-ion-beam milled on a large aluminum grain, and after compression testing and recording the proof strength, the entire specimen with the micropillars were cold-

rolled to a higher pre-strain, and then pillar milling and compression testing were repeated. This sequence was repeated twice for different pre-strains of 7% and 15% shown in Fig. 2, and Fig. 3(b) shows the size dependence of strength measured from the micro-pillars. It can be seen that the size exponent m decreases from 0.98 for no pre-strain, to 0.62 for 7% pre-strain, and then to 0.51 for 15% pre-strain. At each pre-strain, the dislocation microstructure in the master microstructure was imaged by transmission electron microscopy and was digitized, and was then analyzed by the box-counting method as shown in Fig. 3(a). Here, the box-counting dimension Λ_B is for a 2D projection (the TEM image) of a 3D microstructure, and hence it is bounded by $1 < \Lambda_B < 2$, instead of the [2,3] bounds for q mentioned above. Nevertheless, it can be seen that as the pre-strain increases from 0% to 7% and then to 15%, Λ_B increases from 1.52 to 1.62 to 1.78. Thus, on increasing pre-strain, *m* decreases while the fractal dimension Λ_B (or q) increases. The inverse relation between *m* and q in eqn. (4) is thus verified, at least in a qualitative way. The most important conclusion is that the size exponent *m* in eqn. (4) is not a material constant, because for the same material (e.g. Al in Figs. 2 and 3), different *m* values can be obtained, depending on the pre-strain and hence the initial dislocation configuration of the master microstructure.

3. Polycrystalline Microstructures

We discuss next the role of polycrystalline microstructures in affecting strength and deformation of micro-scaled specimens [34]. To illustrate what could be of interest, we consider the issue of whether the Hall-Petch relation would hold for micron-sized specimens with a few grains across the specimen thickness. Fig. 4 shows examples of this category. In this experiment, Ag micro-wires with an initial thickness of ~ 50 μm (Fig. 4(a)) were heat treated to obtain different grain sizes, and these wires were then etched by acid to thinner thickness, followed by tensile testing to determine their strength [32]. Fig. 4(a,b) shows two examples of the polycrystalline microstructure, and Fig. 5(a) shows the Hall-Petch plots, i.e. strength vs (grain size)$^{-1/2}$, of such micro-wires. As a comparison, the Hall-Petch plots of bulk nickel foils with thickness in the millimeter scale are also shown in Fig. 5(b). In both cases of micro- and bulk specimens, the strength deviates from the Hall-Petch trend for the polycrystalline state where there three or fewer grains across the specimen thickness, i.e. when the specimen thickness-to-grain size ratio $t/d \lesssim 3$. For bulk-scale specimens in Fig. 5(b), the deviation is a negative one, which has been understood to be due to the fact that grains that are exposed to the specimen free surfaces are softer, and when t/d is small, such soft surface grains are present in large quantities, so that the overall strength becomes lower [33]. However, for specimens with thickness *t* in the micro-scale (Fig. 5(a)), the deviation from the Hall-Petch trend for $t/d \lesssim 3$ becomes positive. In this case, the surface grains that are present in large quantities for $t/d \lesssim 3$ are stronger, not softer, than the interior grains.

Dislocation-density measurements in fact showed that dislocations in such micron-wires do not accumulate when the t/d ratio is low [35]. Fig. 6(a,b) show the deformed dislocation

microstructures of two Ag micro-wires with t/d ratio of 1.2 and 7.8, respectively, at comparable tensile elongations and initial dislocation contents. It can be seen that for the case of $t/d \approx 1.2$ (Fig. 6(a)), the deformed dislocation density remains at a low value of $\sim 3 \times 10^{14}$m^{-2} compared to the initial dislocation density of $\sim 2 \times 10^{14}$m^{-2}, but for the high t/d ratio case of 7.8 (Fig. 6(b)), the dislocation density increased significantly to $\sim 1 \times 10^{16}$m^{-2} after deformation. Micro-samples with low t/d ratios approaching unity are obviously similar to single-crystalline micro-pillars for which the size effect in eqn. (1) is valid, where dislocations can easily zip out of the free surfaces during deformation instead of accumulate. Hence, in a micro-wire with a low t/d ratio, grains that are exposed to free surfaces should be in a dislocation starved state and so they are stronger than any interior grains present.

DDD simulations have been proven useful in providing conceptual understanding of the grain-boundary effects discussed above. Fig. 7(a) shows Hall-Petch plots simulated using 2D DDD for different specimen thickness *t* in the micron range, and different t/d ratios, with the initial dislocation density at ~10^{13} m^{-2} which is a realistic value [36]. In such 2D DDD models, grains are assumed to occupy a rectangular grid structure with periodic boundary conditions along the tensile direction (the direction perpendicular to the specimen thickness direction) as shown in the selected cases in Fig. 7(b-e). In general, in Fig. 7(a), the positive deviation from the polycrystalline Hall-Petch behavior for small t/d ratios as seen in Fig. 5(a) is successfully predicted. Fig. 5(a) in fact also indicates that, in the regime when strength exhibits positive deviation from the polycrystalline Hall-Petch behavior, a "smaller being stronger" size effect occurs, namely, the smaller the specimen size *t* the larger is the strength. This size effect is of a similar genre as that depicted by eqn. (1), and is also predicted by the simulations in Fig. 7(a). Figs. 7(b-e) show selected cases of different values of *t* and t/d ratio. It can be seen that for $t/d \gtrsim 3$ (Fig. 7(b)), surface grains are subjected to lower stress and are therefore softer than interior ones, because of less dislocation pile-up and lower dislocation density there. Since smaller samples have relatively more surface grains, they are therefore weaker. For $t/d \lesssim 1$ (Figs. 7(c-e)), since grain boundaries are scarce, dislocation pile-up is less which leads to a reduced Hall-Petch slope. Also, as can be seen by comparing Figs. 7(d,e), a smaller sample (Fig. 7(e)) contains fewer dislocations due to the ease of zipping out, and so it is stronger. The simulations here therefore also confirm the experimental observation in Fig. 6(a) where dislocations do not accumulate when t/d is small.

This phenomenon of Hall-Petch deviation illustrates the intricate coupling effects of the internal length scale (the grain size) and the external specimen size in affecting strength.

4. Precipitate Microstructures

As the last microstructure to illustrate, we consider precipitates. A classical precipitated alloy is duralumin which is essentially an Al-Cu-Mg-Mn alloy. Fig. 8 shows the master microstructures of duralumin at two aged conditions, namely, naturally (room-temperature) aged and peak-aged conditions. Precipitated phases including T-phase $Al_{20}Cu_2Mn_3$ and S-phase

Al_2CuMg can be seen. Fig. 9(a) shows the 2% proof strength of duralumin micro-pillars under compression [37, 38]. Remarkably, duralumin exhibits a non-monotonic size effect, in which strength first decreases and then increases on increasing size. The size dependence of strength of precipitated alloys is more complex than the common "smaller-being-stronger" size effect in eqn. (1).

The behavior in Fig. 9(a) can be understood by considering the mean free path Λ of dislocations, which is defined as the mean distance traversed by dislocations, before they become trapped by precipitates or annihilated at the free surfaces of the specimen. In a precipitated micro-specimen of size *D*, if a dislocation can escape trapping by precipitates glide through the specimen thickness, then its free path will be *D*. If a dislocation is pinned by some precipitates, its free path will be some *d* which will scale with the precipitate spacing. Let $F(x)$ be the probability that a dislocation is not pinned by precipitates when it has glided a distance x, the mean free path of all mobile dislocations in the specimen will be

$$\Lambda = F(D) \cdot D + [1 - F(D)] \cdot d \tag{5}$$

$F(x)$ is obviously a decreasing function of x, since the longer a dislocation has traveled in a precipitate field, the smaller is the chance that it is not pinned. A simple, convenient form can be $F(x) = \exp(-\alpha x^{\beta})$, where α and β are empirical, positive parameters, and Fig. 9(b) shows the variation of the mean free path with specimen size *D* for different precipitate spacing *d*, for the case of $\alpha = 0.001725$ and $\beta = 3.325$. It can be seen that for specimen size *D* smaller than the size corresponding to the smallest strength in Fig. 9(a), Λ is close to *D* itself which means that most dislocations are not pinned by the precipitates and can glide through the thickness of the specimen. For *D* larger than the size corresponding to the smallest strength, Λ drops on increasing *D* towards a steady value that is simply *d*; in this case, dislocations are increasingly trapped by precipitates. At the size corresponding to the smallest strength, Λ exhibits a maximum, meaning that dislocations can traverse the farthest, corresponding to minimum resistance to deformation. The non-monotonic size effect of strength in Fig. 9(a) is therefore the result of two strengthening mechanisms at play. In the small-size regime, there are not enough precipitates within the specimen thickness to effectively trap dislocations, so the latter glide through the specimen, leaving the specimen in a continuous dislocation-starved state. Strength is high due to the need to nucleate or mobilize dislocations to sustain deformation. On increasing *D*, more and more precipitates are present which can now trap dislocations; the strengthening mechanism here is the conventional precipitation hardening. At the size at which strength is minimum, both strengthening mechanisms are ineffective – this size is too large for dislocation starvation to be effective, and too small to contain enough precipitates to strengthen the specimen. Fig. 10 shows the microstructure of a deformed duralumin micro-pillar close to the size at which strength reaches minimum. It can be seen that across the specimen thickness, there are only a few (~ ten) large, T-phase precipitates, which should not be effective in offering high precipitation hardening. The residual dislocation density is high at ~ 10^{15} m^{-2}, which indicates that dislocation starvation does not happen.

Notwithstanding the above, in the small-size regime when strength is controlled by the dislocation starved condition, the "smaller-being-stronger" size effect is significantly milder than that in pristine Al without precipitates. When the strength vs size relation in this regime is fitted by eqn. (1), the m value is found to be ~0.51 as shown in Fig. 11, compared with the value of ~0.98 for pristine Al without precipitates or pre-straining (Fig. 3(b)). The m value for duralumin is in fact close to pre-strained Al containing a high density of initial dislocations (Fig. 3(b)). In either a precipitated or dense-dislocation microstructure, the small internal microstructural length scale evidently reduce the dependence of strength on specimen size.

DDD simulations again can provide useful insights into the effects of precipitates on size effect of strength. Fig. 12 shows 2D DDD simulation results on the precipitate effects on strength and dislocation storage [39]. Here, the 2D simulation region is rectangular with an aspect ratio of 1:3, with periodic boundary conditions applied along the long axis which is also the tensile axis, and free surfaces are assumed along the short axis. Dislocation velocity is assumed to be proportional to the effective stress comprising the applied stress, elastic interaction between dislocations and resistance due to Taylor hardening. Dislocation nucleation is modeled by dipole sources which operate at critical stresses σ_{nuc} that follow a Gaussian distribution of mean 15 MPa and standard deviation 6 MPa. Dislocation annihilation is modeled by deleting dipoles less than $1b$ wide from the system. Precipitates are positioned according to a Gaussian distribution with average spacing l_{ave} and standard deviation $0.3l_{ave}$. Dislocation-precipitate interactions in reality are 3D events and in the 2D simulation here, they are modeled as three possible scenarios as a dislocation meets a precipitate: (1) If the glide stress is larger than a critical stress σ_c, then the dislocation overcomes the precipitate and moves at a slower speed with the effective stress reduced by σ_c. (2) Else, if the stress normal to the slip plane is larger than a critical stress set to be $3\sigma_c$, then the dislocation has 10% chance to cross slip over the particle. (3) Else, the dislocation is pinned by the precipitate.

Fig. 12(a) shows that for specimen sizes ranging from 1.5μm to 6.5μm, a "smaller-being-stronger" size effect is predicted, which is more prominent for larger precipitate spacing l_{ave}. Two sets of simulated size effect are shown in Fig. 11, and it can be seen that one of these matches the experimental results for duralumin well. Fig. 12(b) shows that, when compared with the pure Al case without precipitates, dislocation accumulation is enhanced by the presence of precipitates, even in the regime where strength is governed by the dislocation starvation mechanism.

5. Perspectives and Conclusion

The above examples all show that, when dense microstructures exist in micro-specimens, the simple "smaller-being-stronger" picture as represented by the power law in eqn. (1) is far from complete. The microstructures may correspond to an internal length scale that may dominate over, or at least couple with, the external specimen-size length scale to control strength and deformation. In such cases, conventional wisdom often becomes invalid. For

example, in the case of polycrystalline, micro-samples of a given specimen thickness *t* in the micro scale, the Hall-Petch relation may break down in the regime $t/d \lesssim 3$, when loss of dislocations to free surfaces becomes significant leading to low dislocation accumulation. Precipitation hardening is another example – in the alloy example in Section 4, when the specimen size is not large compared with the spacing of precipitates, the latter may no longer be effective in blocking dislocations, leading to a much lower strength than the bulk value. Even in the simpler example of the specimen just containing an initial amount of dislocations, the exponent *m* in eqn. (1) may be affected by the initial dislocation network according to eqn. (4). Other microstructures will most likely produce other unusual effects but the literature is critically short of such information and knowledge.

Modeling of size effects when microstructures dominate is another interesting area requiring challenging developments. The DDD simulations shown in Figs. 7, 10 and 11 are sometimes referred to as "2.5D" simulations which are really 2D simulations for infinitely straight dislocations with certain 3D events, such as interactions with precipitates, dislocation generation and cross slip, modeled in *ad hoc* manners in 2D. Currently, 3-dimensional DDD simulations are often used as a convenient tool to model micro-pillar plasticity, since the slow accumulation of dislocations due to the constant loss at free surfaces, especially for very small crystals with low initial dislocation contents [30, 40], is ideal for 3D DDD which cannot handle large quantities of dislocation segments. The incorporation of microstructures will meet two key challenges for the 3D DDD method: (i) the need to model dislocation-microstructure interactions in the simulation, and (ii) enhanced dislocation accumulation which means more efficient simulation codes will need to be developed.

Acknowledgment

Financial support by the Kingboard Professorship Endowment is gratefully acknowledged.

References

[1] R. Dou, and B. Derby: A universal scaling law for the strength of metal micropillars and nanowires. Scripta Mater. 61, 524 (2009).
[2] J.R. Greer, and J.T.M. De Hosson: Plasticity in small-sized metallic systems: Intrinsic versus extrinsic size effect. Prog. Mater. Sci. 56, 654 (2011).
[3] A.H.W. Ngan, L. Zuo, and P.C. Wo: Size dependence and stochastic nature of yield strength of micron-sized crystals: a case study on Ni_3Al. Prof. Roy. Soc. Lond. A462, 1661 (2006).
[4] L. Zuo, and A.H.W. Ngan: Molecular dynamics study on compressive yield strength in Ni_3Al micro-pillars. Philosophical Magazine Letters 86, 355 (2006).
[5] J.R. Greer, W.C. Oliver, and W.D. Nix: Size dependence of mechanical properties of gold at the micron scale in the absence of strain gradients. Acta Mater. 53, 1821 (2005).
[6] J.R. Greer, and W.D. Nix: Nanoscale gold pillars strengthened through dislocation starvation. Phys. Rev. B 73, 245410 (2006).

[7] Z.W. Shan, R.K. Mishra, S.A.S. Asif, O.L. Warren, and A.M. Minor: Mechanical annealing and source-limited deformation in submicrometre-diameter Ni crystals. Nat. Mater. 7, 115 (2008).
[8] T.A. Parthasarathy, S.I. Rao, D.M. Dimiduk, M.D. Uchic, and D.R. Trinkle: Contribution to size effect of yield strength from the stochastics of dislocation source lengths in finite samples. Scripta Mater. 56, 313 (2007).
[9] D.M. Norfleet, D.M., Dimiduk, S.J. Polasik, M.D. Uchic, and M.J. Mills: Dislocation structures and their relationship to strength in deformed nickel microcrystals. Acta Mater. 56, 2988 (2008).
[10] K.S. Ng, and A.H.W. Ngan: Stochastic nature of plasticity of aluminum micro-pillars. Acta Mater. 56, 1712 (2008).
[11] Y. Cui, C. Po, and N. Ghoniem: Controlling strain bursts and avalanches at the nano- to micrometer scale. Phys. Rev. Lett. 117, 155502 (2016).
[12] S.I. Rao, D.M. Dimiduk, T.A. Parthasarathy, M.D. Uchic, M. Tang, and C. Woodward: Athermal mechanisms of size-dependent crystal flow gleaned from three-dimensional discrete dislocation simulations. Acta Mater. 56, 3245 (2008).
[13] J.A. El-Awady, M. Wen, and N.M. Ghoniem: The role of the weakest-link mechanism in controlling the plasticity of micropillars. J. Mech. Phys. Solids 57, 32 (2009).
[14] C. Motz, D. Weygand, J. Senger, and P. Gumbsch: Initial dislocation structures in 3-D discrete dislocation dynamics and their influence on microscale plasticity. Acta Mater. 57, 1744 (2009).
[15] S. Akarapu, H.M. Zbib, and D.F. Bahr: Analysis of heterogeneous deformation and dislocation dynamics in single crystal micropillars under compression. Int. J. Plasticity 26, 239 (2010).
[16] M. Huang, L. Zhao, and J. Tong: Discrete dislocation dynamics modelling of mechanical deformation of nickel-based single crystal superalloys. Int. J. Plasticity 28, 141 (2012).
[17] Y. Cui, P. Lin, Z.L. Liu, and Z. Zhuang: Theoretical and numerical investigations of single arm dislocation source controlled plastic flow in FCC micropillars. Int. J. Plasticity 55, 279 (2014).
[18] Q. Yu, M. Legros, and A.M. Minor: In situ TEM nanomechanics. MRS Bulletin 40, 62 (2015).
[19] P.J. Imrich, C. Kirchlechner, D. Kiener, and G. Dehm: In situ TEM microcompression of single and bicrystalline samples: insights and limitations. JOM 67, 1704 (2015).
[20] R. Maaß, L. Meza, B. Gan, S. Tin, and J.R. Greer: Ultrahigh Strength of Dislocation-Free Ni3Al Nanocubes. Small 8, 1869 (2012).
[21] L.Y. Chen, M-R. He, J. Shin, G. Richter, and D.S. Gianola: Meauring surface dislocation nucleation in defect-scarce nanostructures. Nature Mater. 14, 707 (2015).
[22] H. Bei, S. Shim, G.M. Pharr, and E.P. George: Effects of pre-strain on the compressive stress-strain response of Mo-alloy single-crystal micropillars. Acta Mater. 56, 4762 (2008).
[23] C.R. Weinberger, and W. Cai: Surface-controlled dislocaiton multiplication in metal micropillars. Proc. Nat. Acad. Sci. 105, 14304 (2008).
[24] T.T. Zhu, A.J. Bushby, and D.J. Dunstan: Materials mechanical size effects: a review. Mater. Technol. 23, 193 (2008).
[25] A.H.W. Ngan: An explanation for the power-law scaling of size effect on strength in micro-specimens. Scripta Mater. 65, 978 (2011).
[26] R. Gu, and A.H.W. Ngan: Dislocation arrangement in small crystal volumes determines power-law size dependence of yield strength. J. Mech. Phys. Solids 61, 1531 (2013).
[27] A.S. Schneider, D. Kiener, C.M. Yakacki, H.J. Maier, P.A. Gruber, N. Tamura, M. Kunz,

A.M. Minor, and C.P. Frick: Influence of bulk pre-straining on the size effect in nickel compression pillars. Mater. Sci. Engg. A 559, 147 (2013).
[28] J.A. El-Awady, M.D. Uchic, P.A. Shade, S-L. Kim, S.I. Rao, D.M. Dimiduk, and C. Woodward: Pre-straining effects on the power-law scaling of size-dependent strengthening in Ni single crystals. Scripta Mater. 68, 207 (2013).
[29] P.S. Phani, K.E. Johanns, E.P. George, and G.M. Pharr: A simple stochastic model for yielding in specimens with limited number of dislocations. Acta Mater. 61, 2489 (2013).
[30] J.A. El-Awady: Unravelling the physics of size-dependent dislocation-mediated plasticity. Nature Comm. 6, 5926 (2015).
[31] R. Gu, and A.H.W. Ngan: Effects of pre-straining and coating on plastic deformation of aluminum micropillars. Acta Mater. 60, 6102 (2012).
[32] X.X. Chen, and A.H.W. Ngan: Specimen size and grain size effects on tensile strength of Ag microwires. Scripta Mater. 64, 717 (2011).
[33] C. Keller, E. Hug, and X. Feaugas: Microstructural size effects on mechanical properties of high purity nickel. Int. J. Plasticity 27, 635 (2011).
[34] B. Ehrler, X.D. Hou, T.T. Zhu, K.M.Y. Png, C.J. Walker, A.J. Bushby, and D.J. Dunstan: Grain size and sample size interact to determine strength in a soft metal. Phil. Mag. 88, 3043 (2008).
[35] X.X. Chen, and A.H.W. Ngan: Tensile deformation of silver micro-wires of small thickness-to-grain-size ratios. Mater. Sci. Engg. A 539, 74 (2012).
[36] P.S.S. Leung, and A.H.W. Ngan: Size effect on the strength of micron-sized polycrystals – a dislocation dynamics simulation study. Scripta Mater. 69, 235 (2013).
[37] R. Gu, and A.H.W. Ngan: Size effect on the deformation behavior of duralumin micropillars. Scripta Mater. 68, 861 (2013).
[38] K. Gan, R. Gu, R., and A.H.W. Ngan: The weakest size of precipitated alloys in the micro regime: the case of duralumin. Submitted.
[39] R. Gu, P.S.S. Leung, and A.H.W. Ngan: Size effect on deformation of duralumin micropillars – a dislocation dynamics study. Scripta Mater. 76, 73 (2014).
[40] C. Zhou, I.J. Beyerlein, and R. LeSar: Plastic deformation mechanisms of fcc single crystals at small scales. Acta Mater. 59, 7673 (2011).

Figure Captions

FIG. 1 – 2% proof strength vs residual dislocation density in aluminum micro-pillars of two sizes (a) 5.6 μm and (b) 1.2 μm. Adapted with permission form Ref. [31], Elsevier, 2012.

FIG. 2 – Dislocation structures of aluminum at different pre-strain levels (a) 0%, (b) 7% and (c) 15% (top panels real, lower panels digitized bitmaps). Adapted with permission form Ref. [26], Elsevier, 2013.

FIG. 3 – (a) "Box-counting" fractal analysis of the dislocation networks in the different pre-strained master microstructures corresponding to Fig. 2. (b) Size dependence of proof strength of aluminum micro-pillars milled from different pre-strained master microstructures in FIG. 2. Adapted with permission form Ref. [26], Elsevier, 2013.

FIG. 4 – Silver micro-wires containing a few grains across their thickness: (a) a wire with thickness $t \approx 50$ μm and internal grain size $d \approx 21$ μm, (b) another wire with thickness $t \approx 40$ μm and internal grain size $d \approx 40$ μm, exhibiting a "bamboo" grain structure. Adapted with permission form Refs. [32, 35], Elsevier, 2011.

FIG. 5 – Hall-Petch plots of strength vs (grain size)$^{-1/2}$ for (a) silver polycrystalline micro-wires with specimen thickness t = 20 to 50 μm (reproduced with permission form Ref. [32], Elsevier, 2011), (b) bulk nickel polycrystalline foils with specimen thickness t = 0.5 mm (adapted with permission form Ref. [33], Elsevier, 2011). In both cases, deviation from the Hall-Petch trend for the mean-field behavior occurs when $t/d \lesssim 3$ (d = grain size), i.e. when there are fewer than about three grains across the thickness of the specimen. In the case of bulk specimens (b), the deviation is a reduction compared to Hall-Petch, while for micro-specimens (a), the deviation is an increment.

FIG. 6 – Large-area TEM montages of deformed microstructures in Ag micro-wires. Individual dislocations can be seen at edges of diffraction bend contours. (a) Wire thickness $t \approx 50$ μm and internal grain size $d \approx 40.6$ μm ($t/d \approx 1.2$), with residual dislocation density estimated at $\sim 3 \times 10^{14}$ m^{-2} at 12% elongation. (b) Wire thickness $t \approx 40$ μm and internal grain size $d \approx 5.1$ μm ($t/d \approx 7.8$), with residual dislocation density estimated at $\sim 1 \times 10^{16}$ m^{-2} at 14% elongation. In both cases, the initial dislocation density of the undeformed samples was ~ 2×10^{14} m^{-2}. Adapted with permission form Ref. [35], Elsevier, 2012.

FIG. 7 – 2-dimensional DDD simulations of grain-boundary induced strengthening in micron-sized polycrystals. (a) Simulated proof stress vs (grain size)$^{-1/2}$ plots for different specimen thicknesses t and grain size d, with t/d ratios shown in brackets. (b-e) Simulated stress fields (upper panels) and dislocation plots (lower panels) for selected cases of different specimen thickness t (shown in terms of b underneath each case) and t/d ratio. Rectangular grids (if any) show simulated grain boundaries. Color bar on right of (e) shows relative scale for stress applicable to all cases in (b-e). Adapted with permission form Ref. [36], Elsevier, 2013.

FIG. 8 – Precipitated microstructures in duralumin at (a) naturally (room-temperature) aged and (b) peak-aged conditions. Rod-shaped T-phase $Al_{20}Cu_2Mn_3$ precipitates are present in (a,b), while (b) also exhibits needle-shaped S-phase Al_2CuMg precipitates.

FIG. 9 – (a) 2% proof stress of duralumin micro-pillars vs pillar diameter *D*. (b) Model mean free path of dislocations in a precipitated micro-specimen [38].

FIG. 10 – TEM microstructure of deformed duralumin pillar close to the size at which strength reaches minimum. (a) Longitudinal microstructure of pillar where large T-phase precipitates are seen as dark spots. (b) Close-up of a typical location in the specimen showing high density of residual dislocations. Adapted with permission form Ref. [37], Elsevier, 2013.

FIG. 11 – Smaller-being-stronger size dependence in duralumin in the regime of small specimen size. Beyond this regime, strength increases with size as shown in FIG. 9(a). Reproduced with permission form Ref. [39], Elsevier, 2014.

FIG. 12 – 2D DDD simulation results of precipitate effects on (a) strength and (b) dislocation storage. Reproduced with permission form Ref. [39], Elsevier, 2014.

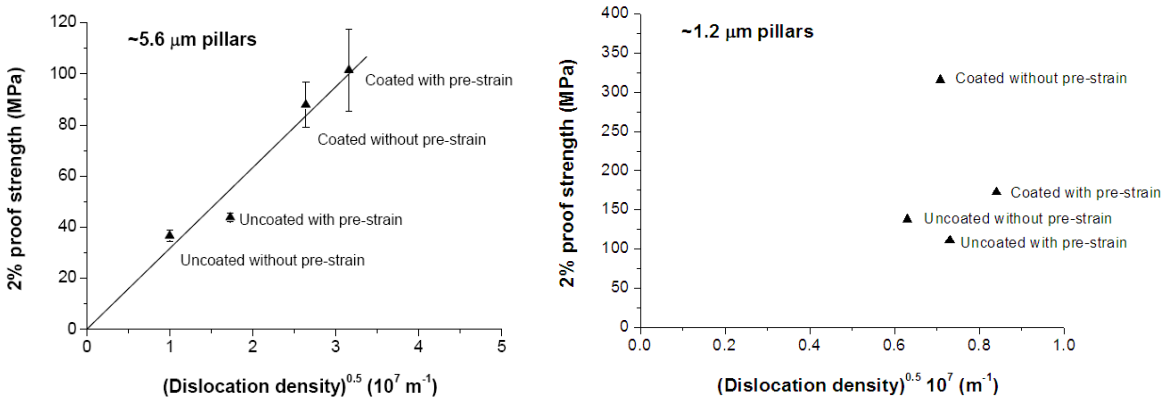

(a) (b)

FIG. 1 – 2% proof strength vs residual dislocation density in aluminum micro-pillars of two sizes (a) 5.6 μm and (b) 1.2 μm. Adapted with permission form Ref. [31], Elsevier, 2012.

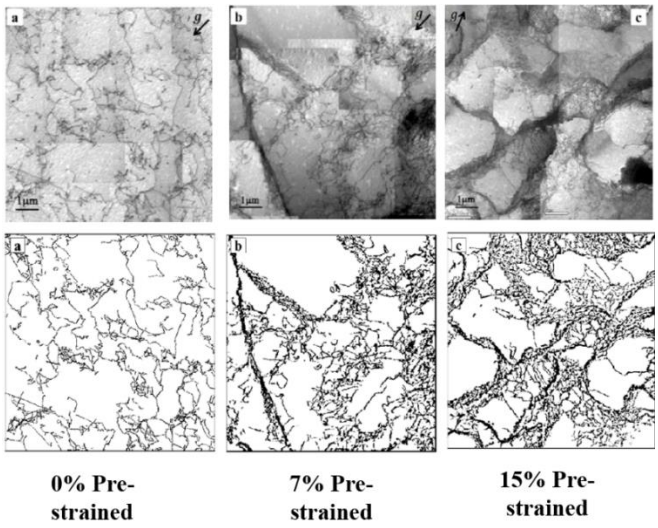

FIG. 2 – Dislocation structures of aluminum at different pre-strain levels (a) 0%, (b) 7% and (c) 15% (top panels real, lower panels digitized bitmaps). Adapted with permission form Ref. [26], Elsevier, 2013.

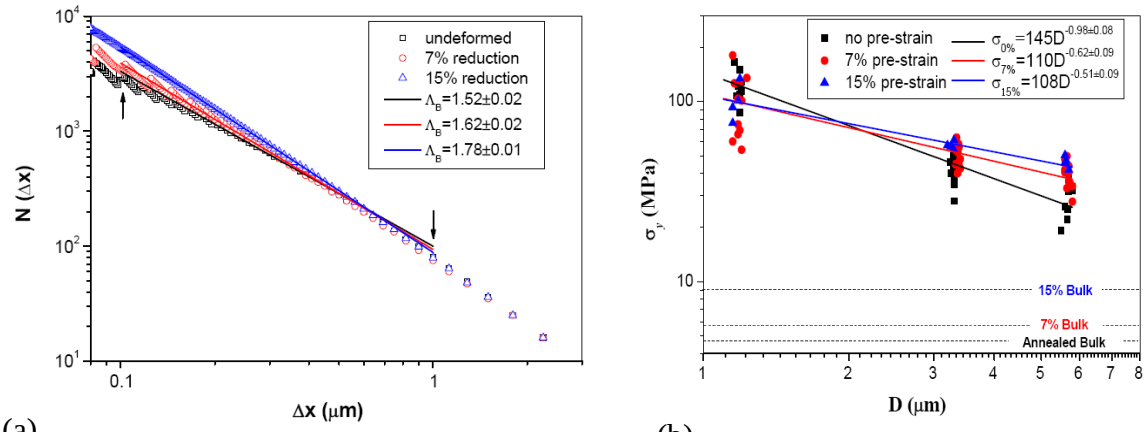

(a) (b)

FIG. 3 – (a) "Box-counting" fractal analysis of the dislocation networks in the different pre-strained master microstructures corresponding to Fig. 2. (b) Size dependence of proof strength of aluminum micro-pillars milled from different pre-strained master microstructures in FIG. 2. Adapted with permission form Ref. [26], Elsevier, 2013.

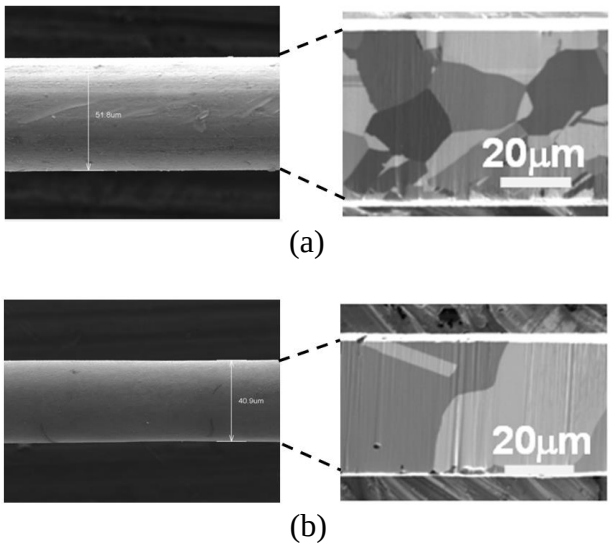

(a)

(b)

FIG. 4 – Silver micro-wires containing a few grains across their thickness: (a) a wire with thickness $t \approx 50$ μm and internal grain size $d \approx 21$ μm, (b) another wire with thickness $t \approx 40$ μm and internal grain size $d \approx 40$ μm, exhibiting a "bamboo" grain structure. Adapted with permission form Refs. [32, 35], Elsevier, 2011.

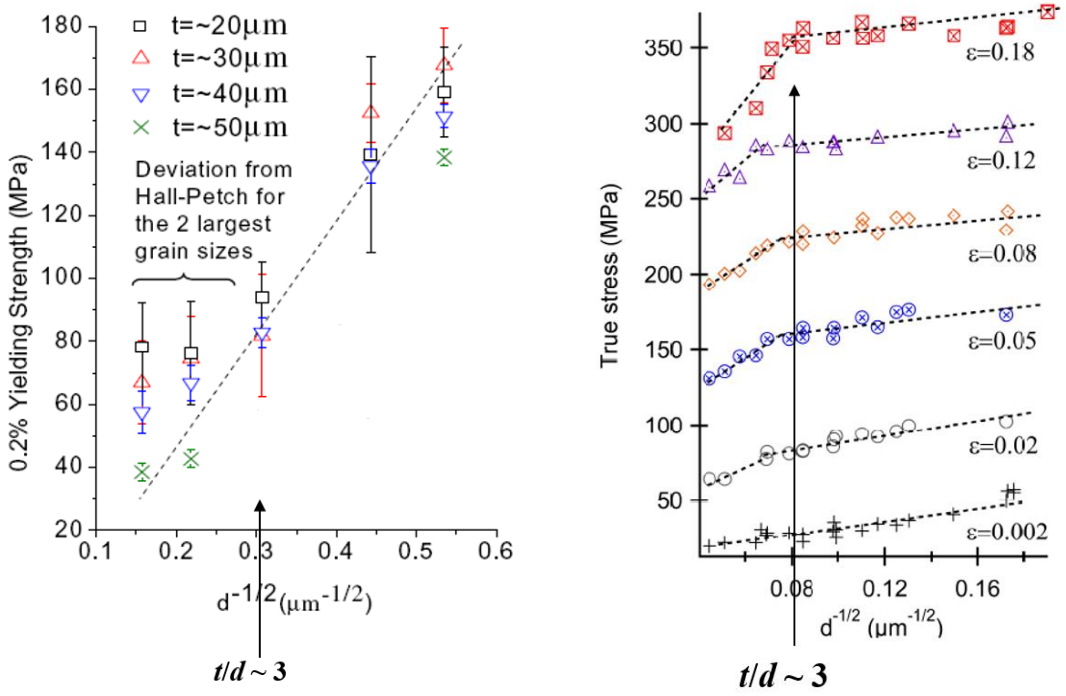

(a) (b)

FIG. 5 – Hall-Petch plots of strength vs (grain size)$^{-1/2}$ for (a) silver polycrystalline micro-wires with specimen thickness t = 20 to 50 μm (reproduced with permission form Ref. [32], Elsevier, 2011), (b) bulk nickel polycrystalline foils with specimen thickness t = 0.5 mm (adapted with permission form Ref. [33], Elsevier, 2011). In both cases, deviation from the Hall-Petch trend for the mean-field behavior occurs when $t/d \lesssim 3$ (d = grain size), i.e. when there are fewer than about three grains across the thickness of the specimen. In the case of bulk specimens (b), the deviation is a reduction compared to Hall-Petch, while for micro-specimens (a), the deviation is an increment.

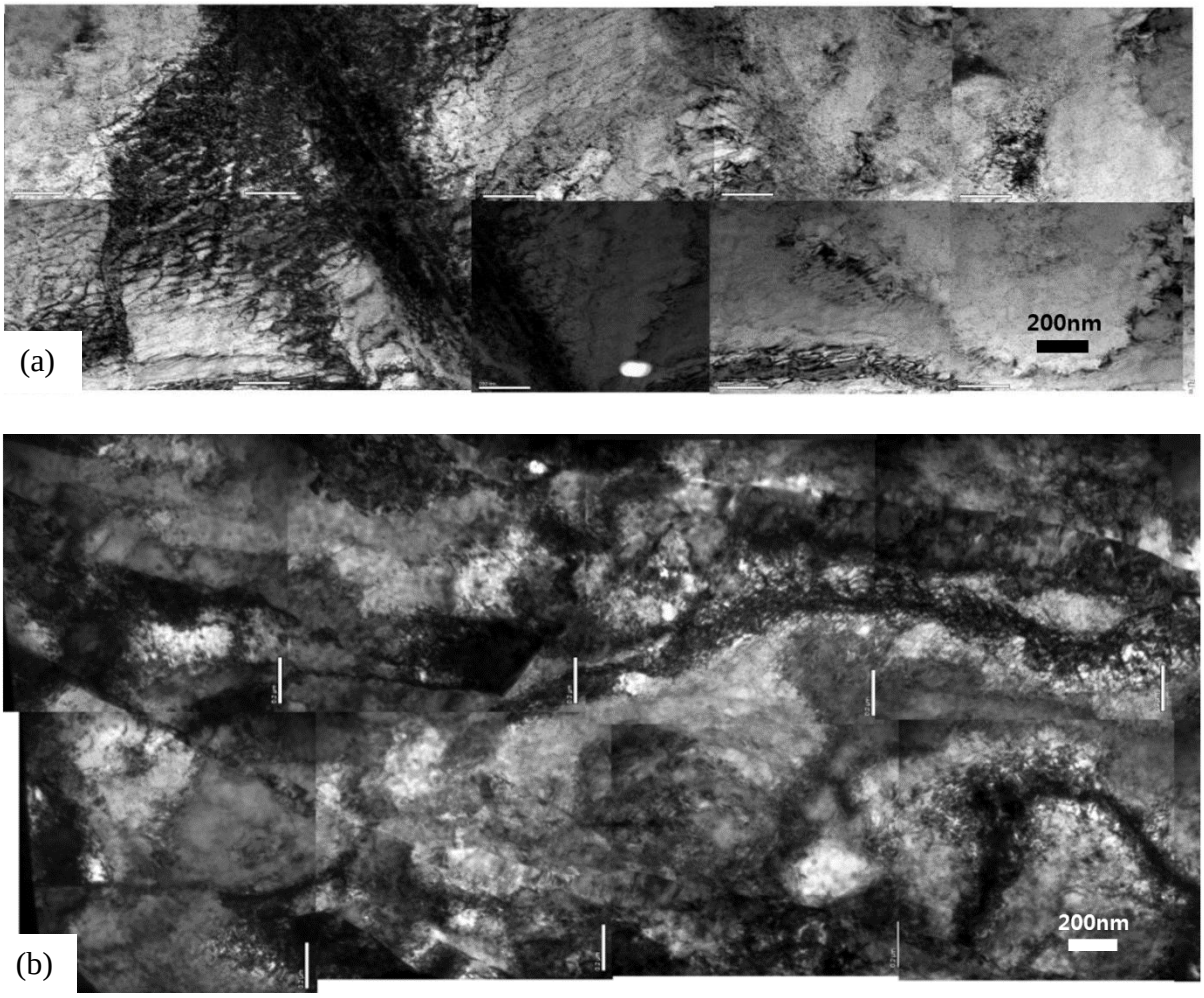

FIG. 6 – Large-area TEM montages of deformed microstructures in Ag micro-wires. Individual dislocations can be seen at edges of diffraction bend contours. (a) Wire thickness $t \approx 50$ μm and internal grain size $d \approx 40.6$ μm ($t/d \approx 1.2$), with residual dislocation density estimated at $\sim 3 \times 10^{14}$ m^{-2} at 12% elongation. (b) Wire thickness $t \approx 40$ μm and internal grain size $d \approx 5.1$ μm ($t/d \approx 7.8$), with residual dislocation density estimated at $\sim 1 \times 10^{16}$ m^{-2} at 14% elongation. In both cases, the initial dislocation density of the undeformed samples was ~ 2×10^{14} m^{-2}. Adapted with permission form Ref. [35], Elsevier, 2012.

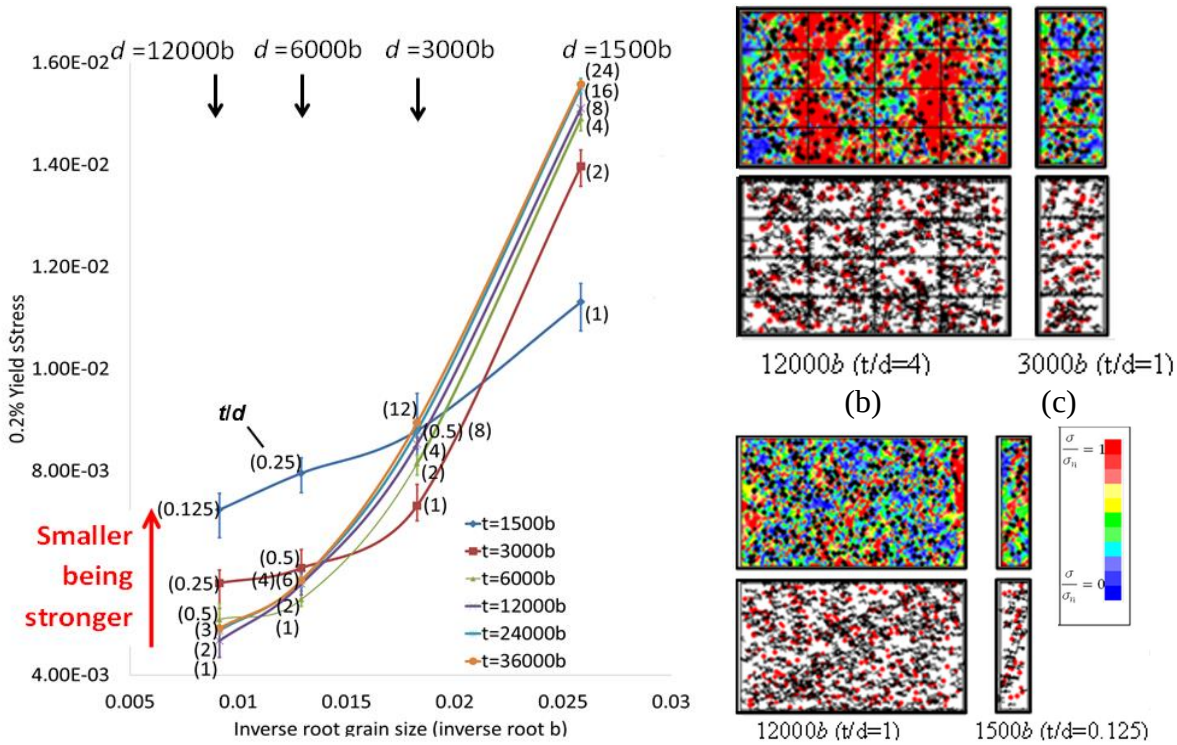

FIG. 7 – 2-dimensional DDD simulations of grain-boundary induced strengthening in micron-sized polycrystals. (a) Simulated proof stress vs (grain size)$^{-1/2}$ plots for different specimen thicknesses t and grain size d, with t/d ratios shown in brackets. (b-e) Simulated stress fields (upper panels) and dislocation plots (lower panels) for selected cases of different specimen thickness t (shown in terms of b underneath each case) and t/d ratio. Rectangular grids (if any) show simulated grain boundaries. Color bar on right of (e) shows relative scale for stress applicable to all cases in (b-e). Adapted with permission form Ref. [36], Elsevier, 2013.

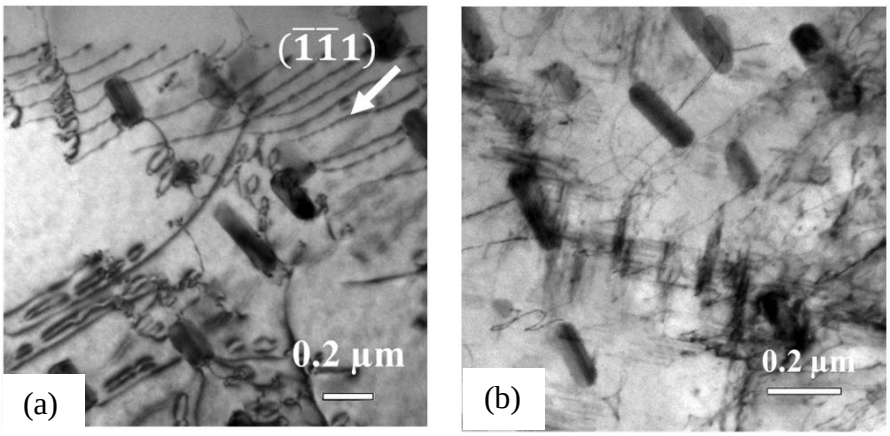

FIG. 8 – Precipitated microstructures in duralumin at (a) naturally (room-temperature) aged and (b) peak-aged conditions. Rod-shaped T-phase $Al_{20}Cu_2Mn_3$ precipitates are present in (a,b), while (b) also exhibits needle-shaped S-phase Al_2CuMg precipitates.

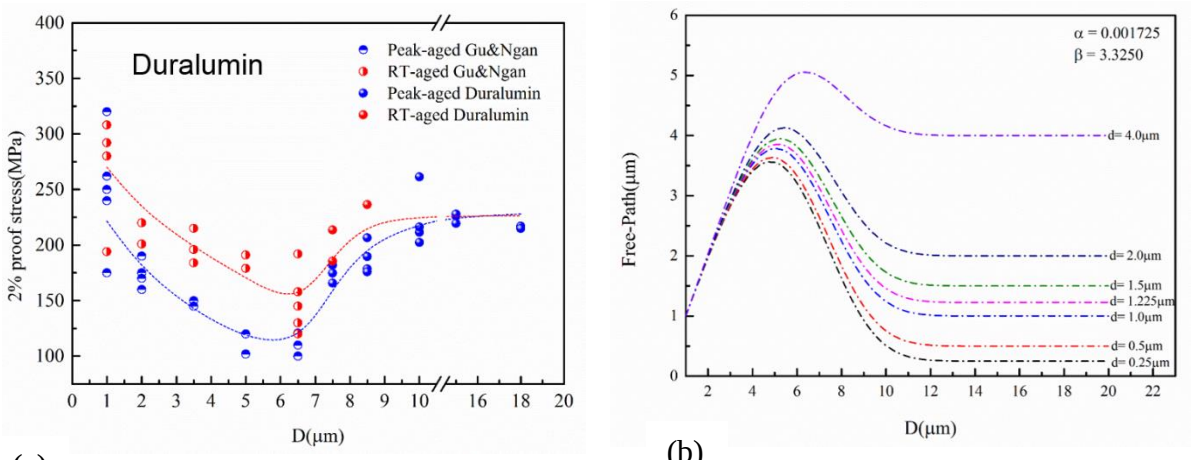

(a) (b)

FIG. 9 – (a) 2% proof stress of duralumin micro-pillars vs pillar diameter *D*. (b) Model mean free path of dislocations in a precipitated micro-specimen [38].

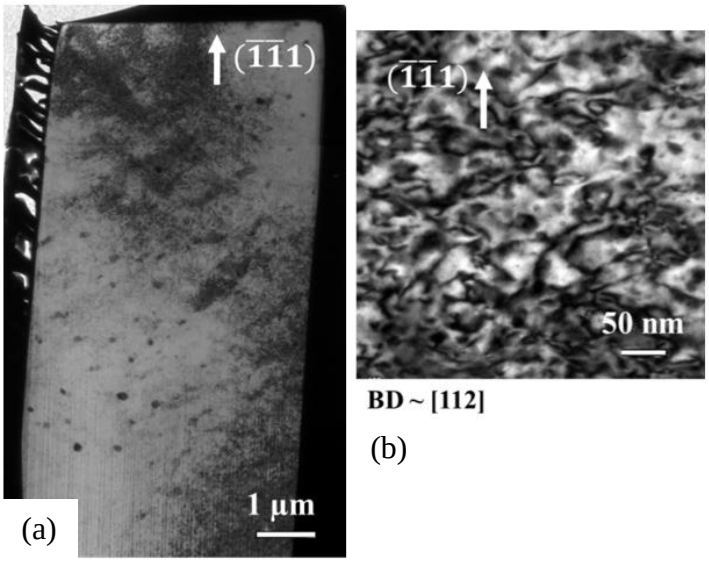

(a) (b)

FIG. 10 – TEM microstructure of deformed duralumin pillar close to the size at which strength reaches minimum. (a) Longitudinal microstructure of pillar where large T-phase precipitates are seen as dark spots. (b) Close-up of a typical location in the specimen showing high density of residual dislocations. Adapted with permission form Ref. [37], Elsevier, 2013.

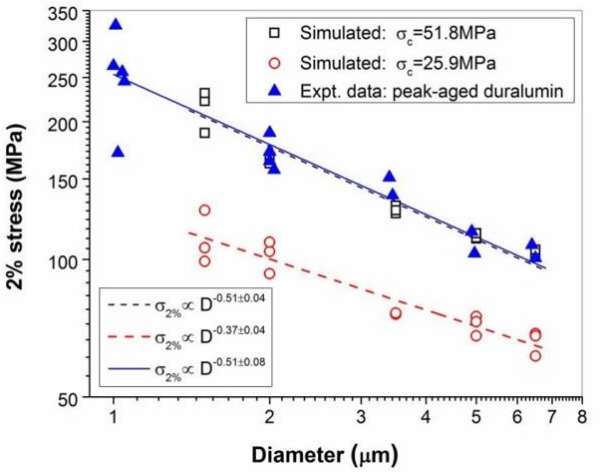

FIG. 11 – Smaller-being-stronger size dependence in duralumin in the regime of small specimen size. Beyond this regime, strength increases with size as shown in FIG. 9(a). Reproduced with permission form Ref. [39], Elsevier, 2014.

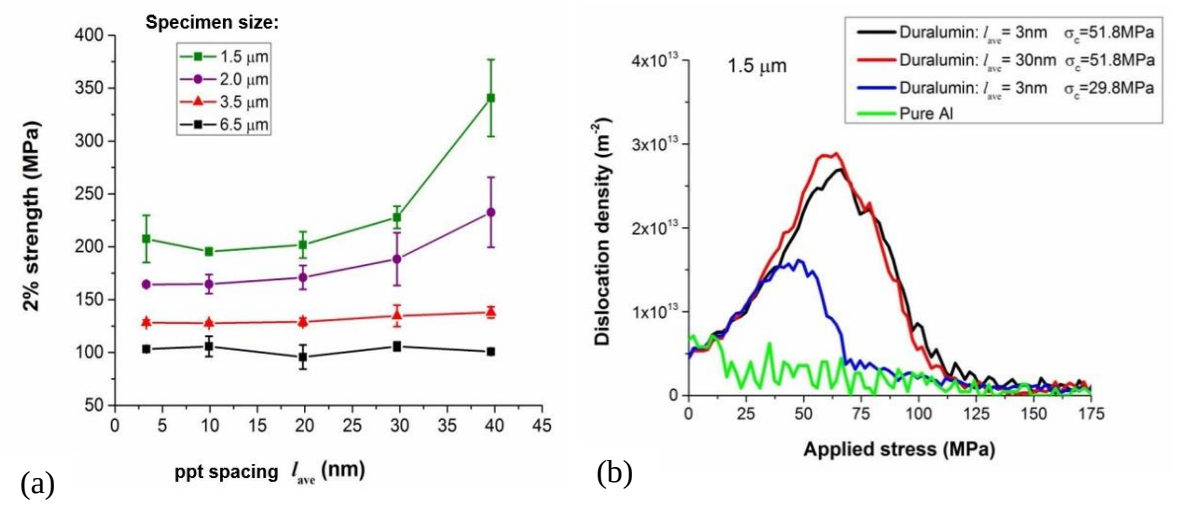

FIG. 12 – 2D DDD simulation results of precipitate effects on (a) strength and (b) dislocation storage. Reproduced with permission form Ref. [39], Elsevier, 2014.